


 Cite this: *RSC Adv.*, 2026, 16, 20544

High-performance activated carbons from *Canarium schweinfurthii* and *Ricinodendron heudelotii* shells for the efficient removal of indigo carmine from water

 Daouda Kouotou, ^{*ab} Frank Dorinel Feudjio Solefack, ^a
 Abdelhakim Elmouwahidi, ^b Murat Yilmaz, ^c Julius Nsami Ndi, ^a
 Agustin F. Perez-Cadenas ^b and Francisco Carrasco-Marin ^b

In this study, two biomass wastes, namely, *Canarium schweinfurthii* shells (CSS) and *Ricinodendron heudelotii* shells (RHS), were converted into activated carbons by chemical activation using phosphoric acid. The two prepared adsorbents were designated as AC-CSS-H₃P and AC-RHS-H₃P, representing the activated carbons derived from CSS and RHS, respectively, through H₃PO₄ activation. The samples were characterized using N₂ adsorption (BET), scanning electron microscopy (SEM), and Fourier-transform infrared (FTIR) spectroscopy analyses. To achieve the removal of indigo carmine (IC) in the batch mode, four adsorption parameters, namely, contact time (5–30 min), pH (2–11), adsorbent dose (10–110 mg), and initial dye concentration (5–25 mg L⁻¹), were thoroughly investigated. Four adsorption isotherms and kinetic models were also evaluated. The specific surface area and pore volume were determined to be 1612 m² g⁻¹ and 0.78 cm³ g⁻¹ for AC-CSS-H₃P and 1696 m² g⁻¹ and 0.90 cm³ g⁻¹ for AC-RHS-H₃P, respectively, with a predominance of acidic functional groups for both samples. After 10 minutes of the contact time with 10 mg of the adsorbent in 100 mL of the IC solution (10 mg L⁻¹), the IC removal efficiency reached approximately 95%. The adsorption of IC was best described by the Langmuir isotherm model, with maximum adsorption capacities of 588 mg g⁻¹ and 1250 mg g⁻¹ for AC-CSS-H₃P and AC-RHS-H₃P, respectively. The pseudo-second-order kinetic model provided the best fit, with correlation coefficients (*R*²) close to unity, indicating a chemisorption mechanism. The adsorption process was predominantly facilitated by hydrogen bonding between the acidic functional groups on the adsorbent surfaces and the anionic form of IC under acidic conditions. Conversely, IC removal decreased in alkaline media due to strong electrostatic repulsion between hydroxide ions and the IC anion. After six regeneration cycles, both adsorbents retained most of their adsorption capacity, demonstrating good reusability. Overall, these results indicate that the activated carbons derived from CSS and RHS are effective adsorbents for the elimination of organic dyes from aqueous solutions.

 Received 21st January 2026
 Accepted 4th April 2026

DOI: 10.1039/d6ra00571c

rsc.li/rsc-advances

1. Introduction

Over the past two decades, dyeing activities have intensified in both artisanal and industrial environments.^{1–6} This increase is largely attributed to the wide availability and use of various natural and synthetic dyes across numerous sectors, including textiles, leather, plastics, printing, food, cosmetics, and

pharmaceuticals.^{7–12} While this industry provides an important source of income for many individuals, it has simultaneously become a global concern due to the significant environmental consequences associated with dye effluents.^{13–17} There is no doubt about the extensive use of dyes in daily life; however, the major concern lies in the large quantities of untreated dye-containing effluents discharged into the environment.^{1,7,8,10} The direct release of dye effluents without prior treatment is considered a poor environmental practice. It poses serious risks to human health and, more critically, to aquatic ecosystems, as dye pollutants reduce the light penetration into water bodies, significantly limiting photosynthesis and consequently causing substantial ecological damage.^{11–16,18,19} Synthetic dyes, even at low concentrations, are challenging to biodegrade because of their intricate aromatic structures, which provide significant

^aApplied Physical and Analytical Chemistry Laboratory, Department of Inorganic Chemistry, Faculty of Science, University of Yaoundé I, PO. Box 812, Yaoundé, Cameroon. E-mail: kouotoudaouda@gmail.com

^bMateriales Polifuncionales Basados en Carbono (UGR-Carbon), Departamento de Química Inorgánica, Unidad de Excelencia Química Aplicada a Biomedicina y Medioambiente, Universidad de Granada (UEQ-UGR), ES18071 Granada, Spain

^cDepartment of Chemistry and Chemical Processing Technologies, Osmaniye Korkut Ata University, PO Box 80010, Osmaniye, Turkey



physicochemical, thermal, and optical stability. These characteristics allow the dyes to persist in wastewater, posing a continuous risk to human and animal health if not properly removed.^{10–14,20} Moreover, many dyes have been reported to exhibit mutagenic and carcinogenic properties, along with other adverse health effects.^{1,8,10–12} Among these hazardous dyes, IC (acid blue 74) is widely used in the textile industry and related sectors.^{4–6,15–17} The selection of IC for this study is particularly relevant, as the global demand for dyed denim fabrics continues to rise, especially in African countries. Consequently, large quantities of IC-containing effluents are discharged into the environment by textile industries, creating increasing environmental and public-health concerns.^{4,10–14,16,17,21,22} The widespread use of the IC dye in the textile industry is largely attributed to its chemical properties. IC is an anionic dye containing two sulfonic groups, which enhance its solubility in water and other solvents by promoting interactions with hydroxyl-containing fibers.^{10–15} If the IC dye is not effectively removed from domestic or industrial effluents, it can persist in aquatic systems, continuously contaminating surface waters and potentially infiltrating groundwater.^{5,11,13,23–25} Therefore, given their recognized harmful effects on the environment, it is imperative to treat IC-contaminated effluents prior to discharge.

To safeguard water resources, numerous efforts have been undertaken to address IC dye pollution, as documented in scientific reports.^{10–13,21,23–25} These initiatives aim to significantly reduce dye concentrations to levels deemed acceptable by the WHO and other environmental organizations. Similarly, various adsorbents have been employed to mitigate IC dye pollution, including carbon-based materials,^{5,6,10–13,22,24,26} clay materials,¹⁵ and activated carbon.^{12,14,21,23,27–33} Currently, several methods have been implemented to remove colored compounds, including chemical and physicochemical approaches such as coagulation and flocculation,³⁴ reverse osmosis,³⁵ photochemical degradation,^{36–39} membrane filtration,^{40,41} and adsorption.^{4,10–12,14,16,17,21–23,29,30,42} Among the adsorbents and remediation methods, adsorption by activated carbons (ACs) is considered the most efficient, eco-friendly, and economic. Their main advantages include flexible design, simple preparation, and convenient operation, in contrast to other methods, which are often costly and require large amounts of chemical reagents.^{10–12,14,21,43–46} There is also growing interest in using renewable biomass residues for the preparation of activated carbons. Biomass residues are abundant, readily available, and serve as excellent precursors for producing ACs with desirable physicochemical properties, which are particularly effective for dye removal.^{12,21,23,27,28,47–49}

Building on the aforementioned considerations, the present study focuses on the use of two biomass wastes, *Canarium schweinfurthii* shells (CSS) and *Ricinodendron heudelotii* shells (RHS), which have been scarcely explored as precursors, for activated carbon production. These biomass residues are abundant in subtropical countries such as Cameroon, where they are generated in large quantities. Moreover, CSS and RHS possess favorable characteristics for adsorbent preparation, including high availability and low ash content, making them

suitable precursors for AC synthesis.^{23,50,51} Furthermore, the chemical activation of lignocellulosic precursors, particularly with phosphoric acid, enhances their mesoporosity, which is advantageous for the adsorption of large dye molecules.^{52,53} Given the chemical structure of IC dye, it qualifies as a large molecule and is therefore suitable for removal using such mesoporous activated carbons. The originality of this work lies in two aspects. First, it utilizes two different lignocellulosic precursors that undergo an acid pretreatment prior to chemical activation under mild-temperature conditions. Second, the resulting activated carbons are employed for the removal of IC dye, an application that has been scarcely explored using these types of biomass waste. Therefore, the overall objective of this study is to add value to these two precursors by converting them into activated carbons and evaluating their adsorption performance for IC dye in aqueous solutions.

2. Materials and methods

2.1. Chemicals

IC dye, or acid blue 74, has a chemical formula of $C_{16}H_8N_2Na_2O_8S_2$, a color index of 73 015, and a molecular weight of $466.35 \text{ g mol}^{-1}$. It was purchased from Sigma-Aldrich Chemie GmbH. Its chemical structure is shown in Fig. 1. Other chemicals, including sulfuric acid (95%), sodium hydroxide (85.5%), hydrochloric acid (37%), and phosphoric acid (85%), were obtained from AnalaR NORMAPUR. All compounds were of analytical quality and utilized without additional purification.

2.2. Activated carbon preparation

Exactly 10 g of each precursor (CSS and RHS, sieved to $800 \mu\text{m}$) was mixed with 7 M H_2SO_4 and subjected to reflux heating at $80 \text{ }^\circ\text{C}$ for 8 hours. Each pretreated sample was then washed and oven-dried at $110 \text{ }^\circ\text{C}$ for 24 hours. The pretreated samples were subsequently impregnated with H_3PO_4 at a mass impregnation ratio of 3 : 2 and oven-dried at $110 \text{ }^\circ\text{C}$ for an additional 24 hours. Following impregnation, a specific quantity of each sample was placed in the reactor of a tubular furnace (CARBOLITE 1200 $^\circ\text{C}$ tube furnace, KEISON Products) and heated at a rate of $5 \text{ }^\circ\text{C min}^{-1}$ to a final temperature of $450 \text{ }^\circ\text{C}$, maintained for 2 hours under a nitrogen flow at 100 mL min^{-1} , and then allowed to cool completely in the furnace. The pyrolyzed samples were initially rinsed with hot water and then with distilled water until the effluents attained neutral pH. The washed samples were then oven-dried at $110 \text{ }^\circ\text{C}$ for 24 hours. After drying, the activated carbon samples were removed from the oven, crushed

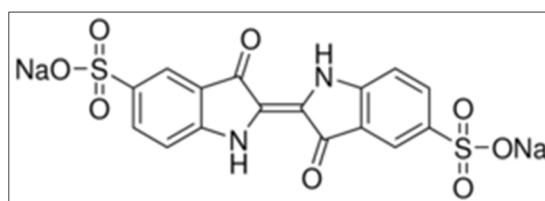


Fig. 1 Chemical structure of IC.



into powders, and stored in glass bottles for further use. The samples were designated as AC-CSS-H₃P and AC-RHS-H₃P, representing activated carbons derived from CSS and RHS *via* H₃PO₄ activation, respectively.

2.3. Characterization of activated carbons

Surface and volume characteristics were determined by N₂ adsorption–desorption using a Micromeritics ASAP 2020 analyzer. The specific surface area was determined using the BET method, the pore volume using the Dubinin–Radushkevich method, and the pore size distribution using the QSDFT method. The surface morphology was investigated using scanning electron microscopy (SEM, JEOL JSM-IT200), and the functional groups on the activated carbon surfaces were subjectively assessed *via* Fourier transform infrared (FTIR) spectroscopy (Vertex 70 DTGS).

2.4. Adsorption experiments

Batch adsorption experiments of IC onto AC-CSS-H₃P and AC-RHS-H₃P were performed by altering the contact time, pH, adsorbent mass, and initial dye concentration to investigate adsorption isotherms and kinetics. The IC stock solution was prepared by dissolving 100 mg of the IC powder in 1000 mL of distilled water, and working solutions were subsequently prepared by dilution. All adsorption experiments were performed at room temperature (23 °C). The IC concentration in the solution was determined using a calibration curve obtained from absorbance measurements of standard IC solutions at $\lambda_{\max} = 614$ nm using a UV-vis spectrophotometer (DR 5500). The amount of IC adsorbed was calculated from the solution concentrations before and after adsorption, expressed as the quantity adsorbed at equilibrium (Q_e), at time t (Q_t), and as the percentage removal (% removal), using the respective equations given below:

$$Q_e = \frac{V \times (C_0 - C_e)}{m}, \quad (1)$$

$$Q_t = \frac{V \times (C_0 - C_t)}{m}, \quad (2)$$

$$\% \text{ Removal} = \frac{(C_0 - C_e)}{C_0} \times 100, \quad (3)$$

where C_0 , C_e , and C_t (mg L⁻¹) represent the initial, equilibrium, and time-dependent concentrations of IC, respectively; V (L) denotes the volume of the IC solution; and m (g) signifies the mass of the adsorbent (AC-CSS-H₃P or AC-RHS-H₃P).

2.5. Adsorption isotherm models

The experimental results were analyzed using four established isotherm models: Langmuir, Freundlich, Temkin, and Dubinin–Radushkevich (D–R). The equations for these isotherms, in their linear forms, are presented in Table 1.

Here, C_e (mg L⁻¹) denotes the equilibrium concentration, Q_m (mg g⁻¹) represents the maximum monolayer adsorption capacity, and K_L (L mg⁻¹) signifies the Langmuir constant related to the adsorption energy. The parameters Q_m and K_L are obtained from the plot of $1/Q_e$ versus $1/C_e$. In addition, the dimensionless separation factor, R_L , serves to assess the viability of adsorption⁶⁰ and is calculated using the following equation:

$$R_L = \frac{1}{1 + K_L C_0}, \quad (4)$$

where C_0 (mg L⁻¹) represents the initial solute concentration. For the Langmuir separation factor, R_L , $R_L = 0$ indicates irreversible adsorption, $0 < R_L < 1$ indicates favorable adsorption, $R_L = 1$ corresponds to linear adsorption, and $R_L > 1$ indicates unfavorable adsorption. For the Freundlich isotherm, K_F (mg g⁻¹) denotes the Freundlich constant, representing the adsorption capacity, and $1/n$ indicates the adsorption intensity. The graph of $\ln Q_e$ versus $\ln C_e$ is utilized to ascertain the Freundlich constants K_F and n . For the Temkin isotherm model, B (J mol⁻¹) represents the heat of adsorption, K_T (L g⁻¹) is the Temkin equilibrium binding constant, R (8.314 J mol⁻¹ K⁻¹) is the universal gas constant, and T (K) indicates the absolute temperature. The parameters B and K_T are obtained from the plot of Q_e versus $\ln C_e$. For the Dubinin–Radushkevich (D–R) isotherm model, Q_D (mg g⁻¹) is the D–R constant and B_D (mol² kJ⁻²) is related to the mean free energy of adsorption.

Table 1 Adsorption isotherms and their linear transformations

Isotherm models	Linear equations	Parameters	References
Langmuir	$\frac{C_e}{Q_e} = \frac{1}{Q_m K_L} + \frac{C_e}{Q_m}$	Q_m and K_L	54
Freundlich	$\ln Q_e = \ln K_F + \frac{1}{n} \ln C_e$	K_F and n	55 and 56
Temkin	$Q_e = B_T \ln C_e + B_T \ln K_T$	B and K_T	57
D–R	$\ln Q_e = -B_D \varepsilon^2 + \ln Q_D$	B_D and Q_D	58 and 59

Table 2 Adsorption kinetics and their linear transformations

Kinetic models	Linear equations	Parameters	References
PFO	$\frac{1}{Q_t} = \frac{k_1}{Q_1 t} + \frac{1}{Q_1}$	k_1 and Q_1	61 and 62
PSO	$\frac{t}{Q_t} = \frac{1}{Q_2^2 k_2} + \frac{t}{Q_2}$	k_2 and Q_2	63 and 64
Elovich	$Q_t = \frac{1}{\beta} \ln(\alpha\beta) + \frac{1}{\beta} \ln t$	α and β	65
Intraparticle diffusion	$Q_t = k_p t^{1/2} + C$	k_p and C	66



These parameters were determined from the plot of $\ln Q_e$ versus ε^2 , where ε is the Polanyi potential, given by the following equation:

$$\varepsilon = RT \times \left[1 + \frac{1}{C_e} \right]. \quad (5)$$

2.6. Adsorption kinetics models

Adsorption kinetics provide insights into the controlling reaction pathways and the mechanisms involved in the adsorption process. It also allows for the determination and prediction of the rate at which the target pollutant is removed from the medium. In this study, the experimental data were fitted to four classic kinetic models: pseudo-first order (PFO), pseudo-second order (PSO), Elovich, and intraparticle diffusion. The linear representations of these models are summarized in Table 2.

In the pseudo-first-order (PFO) model, Q_1 (mg g^{-1}) and Q_t (mg g^{-1}) represent the adsorption capacity at equilibrium and the amount adsorbed at time t , respectively, while k_1 (min^{-1}) is the PFO rate constant. The parameters Q_1 and k_1 are determined from the plot of $\ln(Q_e - Q_t)$ versus t . In the pseudo-second-order (PSO) model, Q_2 (mg g^{-1}) is the adsorption capacity at equilibrium, and k_2 ($\text{g mg}^{-1} \text{min}^{-1}$) is the PSO rate constant, obtained from the plot of t/Q_t versus t . In the Elovich model, α ($\text{mg g}^{-1} \text{min}^{-1}$) is the initial adsorption rate, and β (g mg^{-1}) is the desorption coefficient; these parameters are determined from the plot of Q_t versus $\ln t$. In the intraparticle diffusion model, k_p ($\text{mg (g min}^{1/2})^{-1}$) is the intraparticle diffusion rate constant, and C (mg g^{-1}) is the intercept reflecting the boundary layer effect; both are obtained from the plot of Q_t versus $t^{1/2}$.

3. Results and discussion

3.1. Characterization results of the precursors, AC-CSS-H₃P and AC-RHS-H₃P

3.1.1. Proximate and elemental analyses. The results of the proximate and elemental analyses of the prepared activated

carbons are summarized in Table 3. According to the proximate analysis, CSS contains 5.23% moisture, 68.07% volatile matter, 4.31% ash, and 22.32% fixed carbon, whereas RHS contains 5.07% moisture, 63.53% volatile matter, 3.25% ash, and 28.15% fixed carbon. According to the elemental analysis, CSS is primarily composed of carbon (61.86%), hydrogen (4.36%), nitrogen (3.05%), and oxygen (30.76%), while RHS contains carbon (60.78%), hydrogen (3.46%), nitrogen (2.95%), and oxygen (33.86%). The ash contents, nitrogen levels, and carbon levels in CSS and RHS are comparatively higher than those reported for coconut shells and shea nut shells, while the other components are similar. The CSS and RHS precursors exhibit low ash contents and high carbon contents, indicating that they are suitable raw materials for activated carbon production.

3.1.2. FT-IR spectra of AC-CSS-H₃P and AC-RHS-H₃P. Fig. 2 presents the FTIR spectra utilized to ascertain the functional groups present on each activated carbon. The spectra indicate that activation induces significant changes in the surface chemistry of the two biomasses, as evidenced by the disappearance of several characteristic bands and the appearance of new ones (Fig. 2a and b). Moreover, both activated carbons display similar functional groups, as reflected by the strong resemblance between their FTIR spectra (Fig. 2c). The bands observed between 900 and 500 cm^{-1} are ascribed to the out-of-plane deformation vibrations of aromatic C-H bonds on the surface of the activated carbons. The FTIR spectra of the materials also exhibit bands at around 1707 cm^{-1} , characteristic of C=O bonds. These bands indicate the presence of carboxylic, ketone, aldehyde, and lactone groups on their surface. Furthermore, the absorption bands at approximately 1175.53 cm^{-1} and 1074.84 cm^{-1} correspond to C-O stretching vibrations, while the bands around 1587.47 cm^{-1} are associated with C=C stretching in aromatic rings. These findings confirm the successful functionalization of the prepared activated carbons and suggest their strong potential to interact with IC molecules through multiple adsorption mechanisms.

3.1.3. SEM results. The microstructures of the prepared activated carbons, as observed by SEM, are presented in Fig. 3.

Table 3 Proximate and elemental analyses of AC-CSS-H₃P and AC-RHS-H₃P

Property	Percentage (wt%)				
	CSS (this study)	RHS (this study)	Sherry stone shells ⁶⁷	Coconut shells ⁶⁸	ASTM test standard
Proximate analysis					
Moisture	5.23	5.07	3.90	5.62	D 1762-84
Volatiles	68.07	63.53	82.78	74.9	D 5832-98
Ash	4.31	3.25	0.40	0.70	D 2866-11
Fixed carbon ^a	22.32	28.15	16.82	24.40	
Elemental analysis					
Carbon	61.86	60.78	52.76	53.90	
Hydrogen	4.36	3.46	6.18	5.70	
Nitrogen	3.05	2.95	0.76	0.10	
Sulphur	n.d. ^b	n.d. ^b	0.02	0.02	
Oxygen ^a	30.76	33.86	40.28	39.44	

^a By difference. ^b No detection.



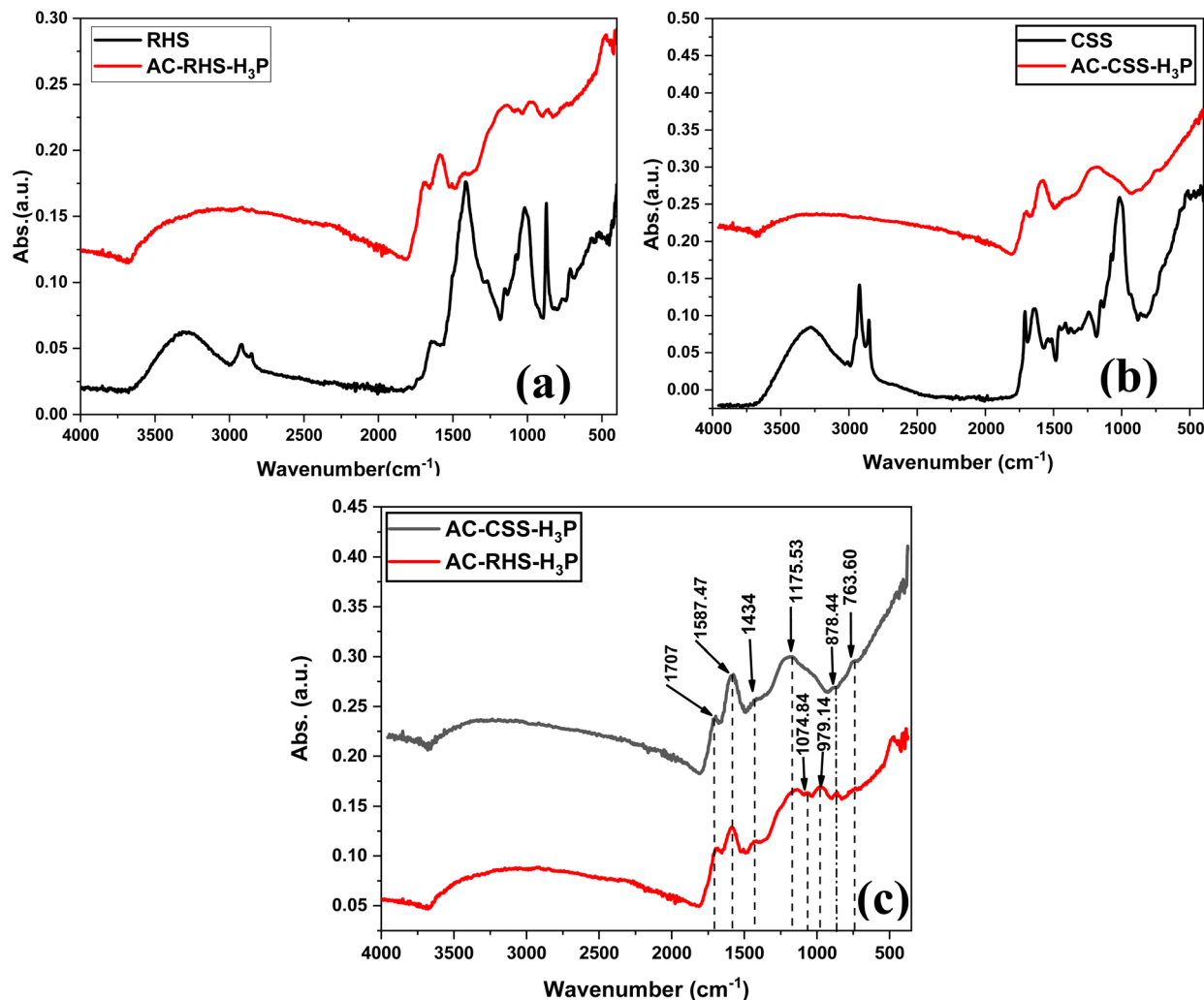


Fig. 2 FT-IR comparison spectra of (a) RHS and AC-RHS-H₃P, (b) CSS and AC-CSS-H₃P, and (c) AC-CSS-H₃P and AC-RHS-H₃P.

Both AC-CSS-H₃P and AC-RHS-H₃P exhibit heterogeneous surface morphologies with the presence of pores of various sizes. This heterogeneity in the pore structure may facilitate the adsorption of IC from the aqueous solution by providing a broad range of adsorption sites and diffusion pathways. In particular, AC-RHS-H₃P appears to possess a more developed porosity than AC-CSS-H₃P, as evidenced by its rougher surface and the predominance of numerous large pores distributed across the carbon matrix. This more extensive pore network is likely to enhance the adsorption capacity of AC-RHS-H₃P toward IC by increasing the available surface area and pore volume accessible to dye molecules.

3.1.4. Nitrogen adsorption–desorption isotherm analysis.

The textural characteristics of the activated carbons were assessed by N₂ adsorption–desorption analysis. Fig. 4 displays the isotherms and pore size distribution curves. Both materials exhibit type I(b) isotherms (Fig. 4a and b), characteristic of adsorbents containing predominantly large micropores and narrow mesopores.⁶⁹ These observations are supported by the high concentration of pore sizes, obtained by the QSDFT method, in the range from 0.45 to 2 nm and a low concentration

in the range from 2 to 4 nm (Fig. 4c and d). Furthermore, according to the isotherms, it appears that the volume of N₂ adsorbed by AC-RHS-H₃P is higher, which could reflect more developed surface and volume properties for this sample. This hypothesis is confirmed by the data shown in Table 4. Indeed, the specific surface area values, obtained using the BET model, are estimated to be 1612 and 1696 m² g⁻¹ for AC-CSS-H₃P and AC-RHS-H₃P, respectively. A similar trend is observed for the specific surface area values obtained by DFT calculations, which are estimated at 1326 and 1504 m² g⁻¹, respectively. It is interesting to note that the experimental specific surface areas of the two coals are relatively similar, which may be due to the fact that the volatile matter contents of the two biomass samples are also similar (68.07% and 63.53%). In addition, AC-RHS-H₃P has a more developed pore volume, with a total volume, $V_{0.95}$ (N₂), of 0.90 cm³ g⁻¹, compared to 0.78 cm³ g⁻¹ for AC-CSS-H₃P, which is consistent with the observations made from the SEM images of the samples. A similar trend is observed with the volumes obtained by DFT calculations. Furthermore, the data presented in Table 4 reveal the microporous nature of the samples. Indeed, the microporous



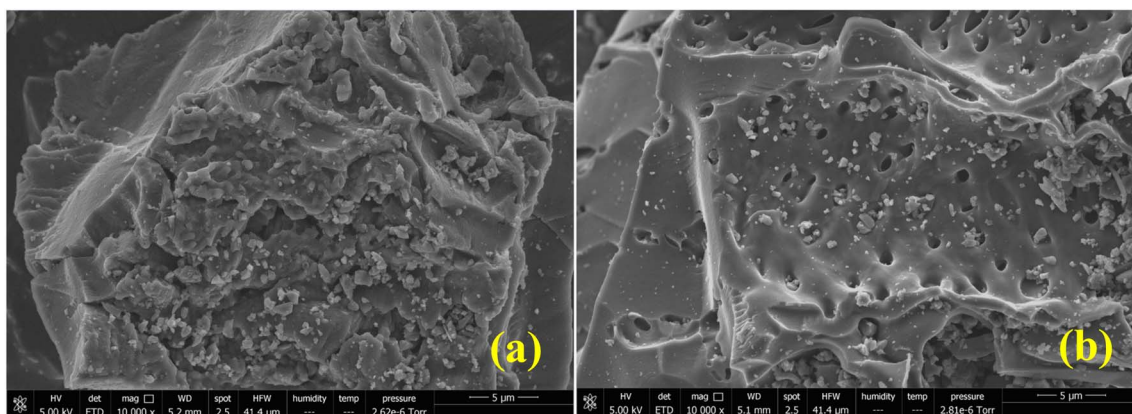


Fig. 3 SEM images of the (a) AC-CSS-H₃P and (b) AC-RHS-H₃P samples.

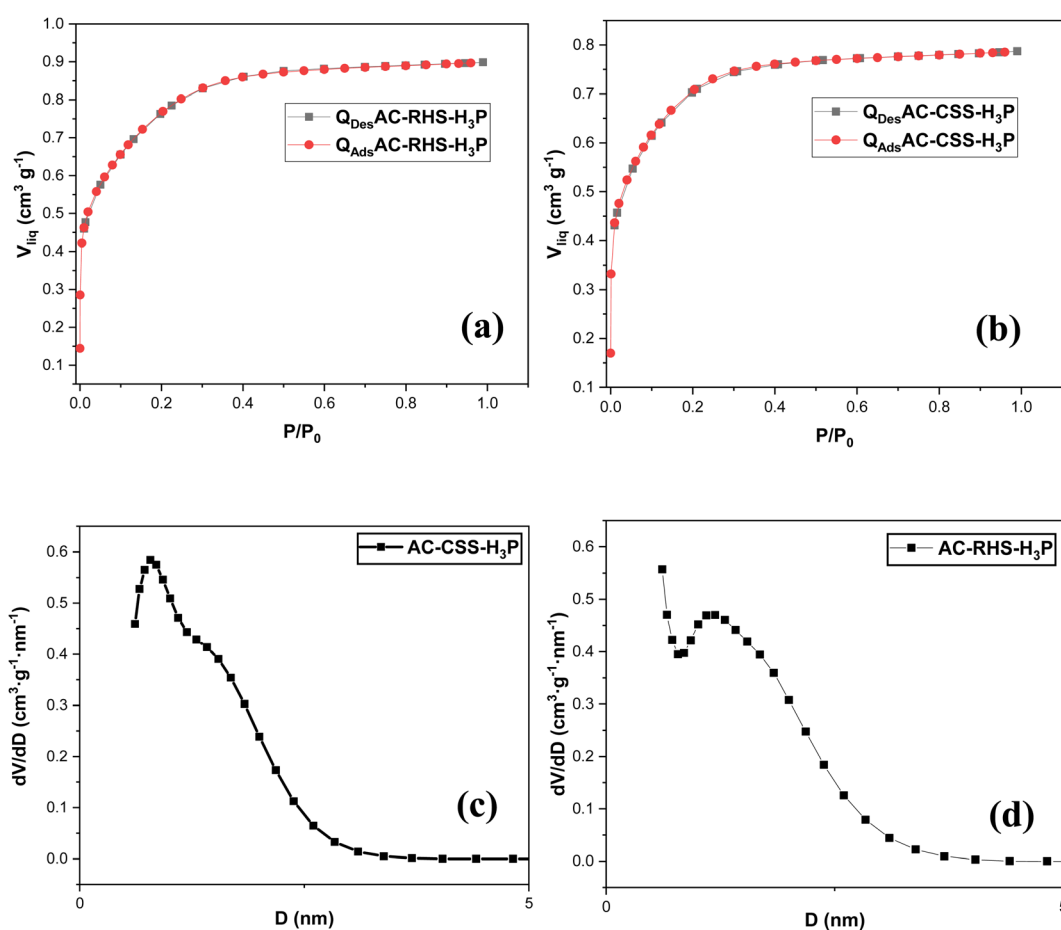


Fig. 4 N₂ adsorption–desorption isotherms (a and b) and QSDFT pore size distribution plots (c and d) of AC-CSS-H₃P and AC-RHS-H₃P.

volumes, W_0 (N₂), cover 75.64% and 66.66% of the total pore volume for the AC-CSS-H₃P and AC-RHS-H₃P samples, respectively. In addition, the analyses estimate that the average pore sizes are 1.43 nm and 1.34 nm, respectively. These results correlate with relatively low mesopore volume values. The more developed surface and volume properties of AC-RHS-H₃P may

afford it a greater predisposition to retain IC molecules from the aqueous solution.

The pH at the point of zero charge (pH_{PZC}) of the activated carbons is determined to be 5.49 and 5.43 for AC-CSS-H₃P and AC-RHS-H₃P, respectively. These pH_{PZC} values, being below 7, indicate a predominance of acidic functional groups on the surface of both adsorbents. Additionally, the similarity in pH_{PZC}



Table 4 Surface characteristics of AC-CSS-H₃P and AC-RHS-H₃P

Sample	pH _{PZC}	S _{BET} (m ² g ⁻¹)	S _{DFT} (m ² g ⁻¹)	W ₀ (N ₂) (cm ³ g ⁻¹)	L ₀ (N ₂) (nm)	V _{DFT} (cm ³ g ⁻¹)	V _{0.95} (N ₂) (cm ³ g ⁻¹)	V _{meso} (N ₂) (cm ³ g ⁻¹)
AC-CSS-H ₃ P	5.49	1612	1326	0.59	1.43	0.72	0.78	0.20
AC-RHS-H ₃ P	5.43	1696	1504	0.60	1.34	0.82	0.90	0.30

suggests that the two materials may exhibit comparable surface charge behaviors across varying pH conditions. Consequently, at solution pH values below the pH_{PZC}, the adsorption of the anionic IC dye onto these activated carbons is expected to be favorable due to the positively charged surface sites.

3.2. Analysis of adsorption parameters

3.2.1. Effect of contact time. To examine the influence of the contact duration, studies were performed across a time span

of 0–30 min utilizing an adsorbent dosage of 10 mg and an initial concentration of IC dye of 10 mg L⁻¹. As shown in Fig. 5a, the adsorption process exhibits three distinct stages. The initial stage is marked by a rapid uptake of IC, due to the plentiful active adsorption sites present.^{70,71} During this stage, a linear increase in IC removal is observed, lasting approximately 5 min. The second stage, occurring between 5 and 10 min, shows a slight reduction in the adsorption rate, which may be due to the progressive occupation of active sites and the decreasing

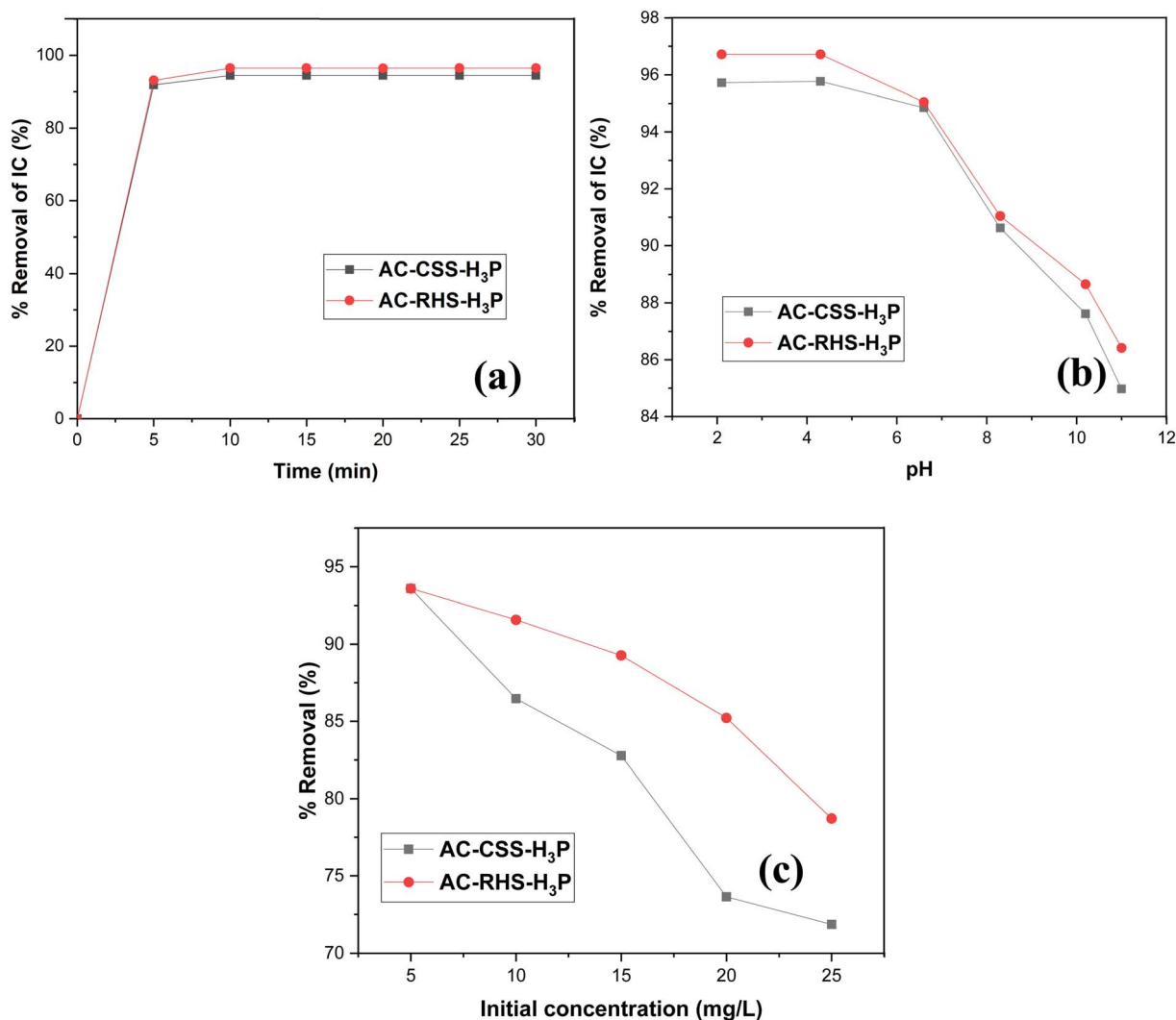


Fig. 5 Analysis of the adsorption parameters: (a) effect of the contact time (adsorbent dose = 10 mg; initial IC concentration = 10 mg L⁻¹, and V = 100 mL), (b) effect of pH (adsorbent dose = 10 mg; initial IC concentration = 10 mg L⁻¹; contact time = 10 min; and pH = 2–11), and (c) effect of the initial IC concentration (pH = 4.0; adsorbent dose = 10 mg; contact time = 10 min; and initial concentration = 5–25 mg L⁻¹) on the percentage removal of the IC dye using AC-CSS-H₃P and AC-RHS-H₃P.



concentration of IC in the solution. The third stage begins after 10 min, where an equilibrium state is achieved, likely due to the saturation of the remaining adsorption sites. At equilibrium, the IC removal efficiencies reach 94% and 96% for AC-CSS-H₃P and AC-RHS-H₃P, respectively. Therefore, 10 min was selected as the optimal equilibrium contact time for the subsequent experiments.

3.2.2. Effect of pH. The experiments to determine the optimal pH for IC dye removal were conducted for a fixed contact time of 10 min at an adsorbent dose of 10 mg while varying the pH from 2 to 11. For each experiment, the pH of the dye solution was adjusted to the desired value before adding the adsorbent and initiating stirring. As shown in Fig. 5b, for both adsorbents, the maximum removal efficiency is achieved in the pH range of 2–4, followed by a slight decrease in removal efficiency at pH values above 5. A similar trend, with the optimum IC removal near pH 2, has been reported by other authors.^{71,72} The high removal efficiency in the acidic pH range (2–4) can be explained by the pH_{PZC} values of the materials (5.43 and 5.49 for AC-CSS-H₃P and AC-RHS-H₃P, respectively). The surface charge of the adsorbents becomes positive below the pH_{PZC} , promoting attraction of the anionic IC dye species, whereas at pH values

above the pH_{PZC} , the surface becomes negatively charged. Consequently, under basic conditions, electrostatic repulsion occurs, limiting IC adsorption and resulting in a reduced removal efficiency.²³ Furthermore, the high removal efficiency observed under acidic conditions can be attributed to the favorable interactions between the adsorbents and IC molecules, particularly through hydrogen bonding between the acidic surface functional groups of AC-CSS-H₃P and AC-RHS-H₃P and the nitrogen- and oxygen-containing functional groups of the IC molecule.^{11,64,73} At $pH > 6.8$, the excess hydroxide ions in the solution impart negative charges to the surface of both activated carbons, leading to electrostatic repulsion with the anionic IC species.¹¹ As a result, the negatively charged surface sites do not favor IC adsorption due to this repulsive interaction.³ In addition, the competition between IC anions and hydroxide ions for the same adsorption sites, coupled with the predominance of weaker van der Waals forces and physical interactions, further contributes to the decrease in removal efficiency under alkaline conditions. Similar observations have been reported by other authors for IC adsorption^{5,11,71,73} and for Congo red adsorption on cashew nut shells.^{3,74}

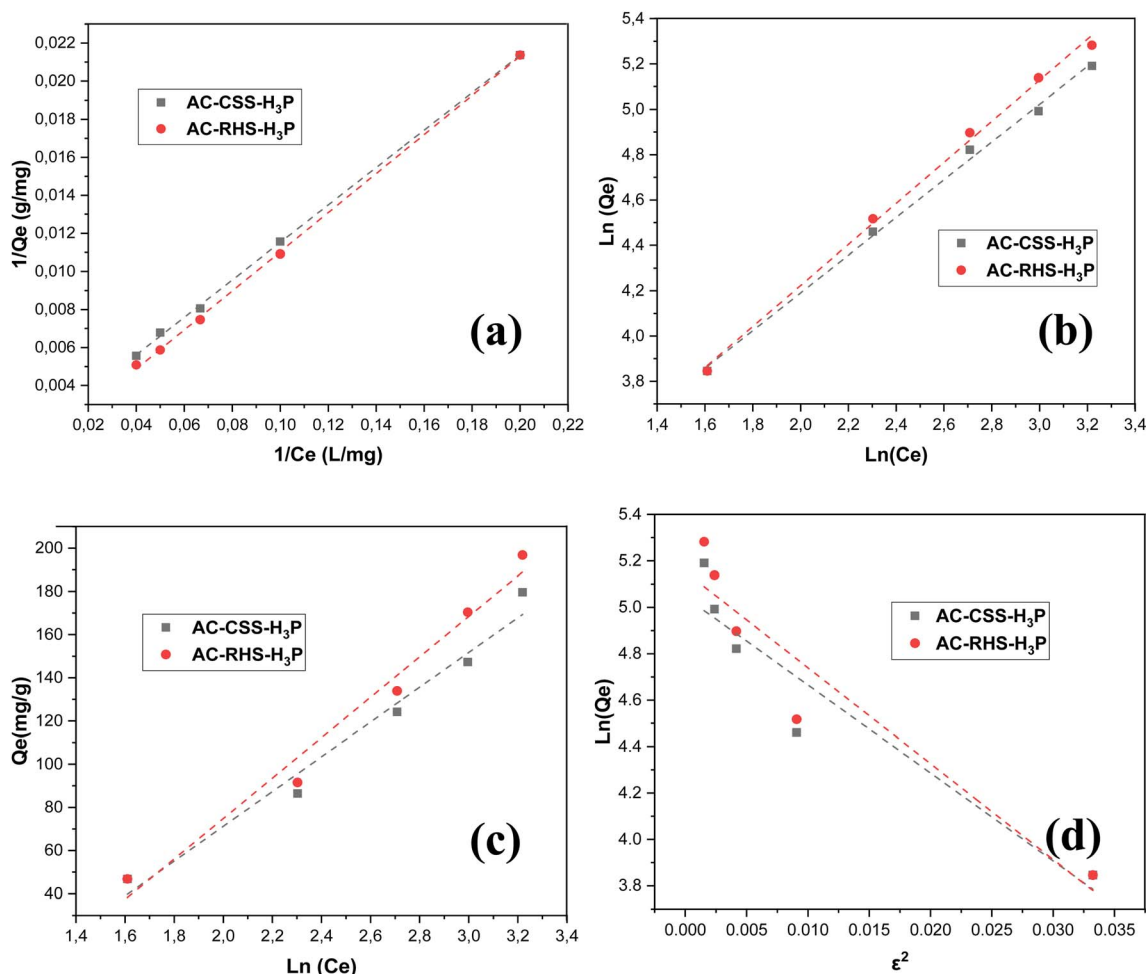


Fig. 6 Isotherm modeling plots of IC removal using AC-CSS-H₃P and AC-RHS-H₃P ($C_0 = 10 \text{ mg L}^{-1}$; contact time = 10 min; mass weight = 10 mg, and $pH = 4.0$): (a) Langmuir model, (b) Freundlich model, (c) Temkin model, and (d) D–R model.



3.2.3. Effect of initial concentration. To evaluate the effect of the initial IC concentration on dye removal, the previously established optimal conditions were applied, namely, an adsorbent dose of 10 mg, a pH of 4.0, and a contact time of 10 min, while the initial dye concentration was varied from 5 to 25 mg L⁻¹. As illustrated in Fig. 5c, the percentage removal of IC decreases with increasing initial dye concentration for both activated carbons, indicating that this parameter significantly influences the adsorption process. Specifically, the removal efficiency decreases from 93.58% to 71.85% for AC-CSS-H₃P and from 93.58% to 78.71% for AC-RHS-H₃P as the initial

concentration increases from 5 to 25 mg L⁻¹. This decline in percentage removal is due to the restricted availability of active sites on the adsorbent surface; as the dye concentration rises, the available sites become saturated, resulting in a lower removal efficiency. At lower concentrations, a greater proportion of dye molecules can access and occupy active sites, leading to higher removal. Similar behavior has been reported by Senthil *et al.*³ for the adsorption of Congo red dye onto cashew nut shells.

3.3. Analysis of adsorption isotherms

The adsorption isotherms were evaluated by fitting the experimental data to the Langmuir, Freundlich, Temkin, and D-R models. Accordingly, the linear plots of $1/Q_e$ versus $1/C_e$, $\ln(Q_e)$ versus $\ln(C_e)$, Q_e versus $\ln(C_e)$, and $\ln(Q_e)$ versus ε^2 for IC adsorption onto AC-CSS-H₃P and AC-RHS-H₃P are presented in Fig. 6. These linear transformations with respect to the equilibrium concentration were employed to determine the corresponding adsorption parameters (Table 5). The adequacy of the experimental data for each adsorption model was evaluated based on the correlation coefficient (R^2). An inspection of Table 5 indicates that the four isotherm models examined fit the experimental data well. A similar observation was reported in our previous work on the adsorption of IC onto cola nut shells.²¹ However, the best fit is observed for the Langmuir model, which yields the highest R^2 value. This model states that the maximum adsorption is achieved when a saturated monolayer of solute molecules covers the adsorbent surface.⁵³ A comparison of the

Table 5 Parameters of the adsorption isotherms

Isotherms	Parameters	AC-CSS-H ₃ P	AC-RHS-H ₃ P
Langmuir	Q_{\max} (mg g ⁻¹)	588.24	1250.00
	K_L (L mg ⁻¹)	0.0162	0.0075
	R_L	0.8606	0.9302
	R^2	0.999	0.999
Freundlich	$1/n$	0.832	0.9048
	K_F (mg g ⁻¹)	0.0799	0.0895
	R^2	0.997	0.997
Temkin	B_T (J mol ⁻¹)	80.547	93.631
	K_T (L g ⁻¹)	3.0527	3.3234
	R^2	0.975	0.978
D-R	B_D (mol ² kJ ⁻²)	41.322	37.905
	Q_D (mol ² kJ ⁻²)	172.8977	155.1202
	E (J mol ⁻¹)	0.1100	0.1149
	R^2	0.907	0.903

Table 6 Comparison of the maximum adsorption capacities of dyes onto other materials

Adsorbents	Maximum adsorption capacities (mg g ⁻¹)	Surface area (m ² g ⁻¹)	Dominant adsorption mechanism	References
Carbon nanotubes	136.00	145.90	Chemisorption	10
CuAl-LDH/SWCNT nanocomposite	297.12	—	—	11
Chitosan/activated carbon composite	208.33	256.82	Physisorption	12
Cobalt hydroxide nanoparticles	163	—	—	13
Montmorillonite	40.00	73.916	—	15
Cola nut shells	10.22	—	Chemisorption	21
Fe-Ni nanostructures	977.18	134.11	Chemisorption	22
ACZ/AgNP	411.68	—	Chemisorption	23
ACZ	121.00	—	Chemisorption	23
Mg/Fe layered double hydroxide nanoparticles	62.80	85.5	Chemisorption	24
Chitosan hydrogel/Hyper-crosslinked polymer particles	118.00	—	—	25
Apricot stone activated carbon	552.55	98	Chemisorption	31
Maize cob carbon	118.48	809.8	Physisorption	32
Commercial activated carbon	298.34	1250.320	Chemisorption	33
Pomegranate peel (APP)	158.73	51.0674	Physisorption	71
Chitosan	500.00	—	Chemisorption	75
Chitosan/ β -cyclodextrin crosslinked bead particles	1000.00	—	Chemisorption	75
Calcined (Zn/Al + Fe) layered double hydroxide	617.3	53.29	—	76
Nanofiber membranes	266.77	140.1	Chemisorption	77
<i>Acacia nilotica</i> (babool) sawdust activated carbon	37.91	—	—	78
Magnesium oxide nanoparticles	559.2	127.442	Chemisorption	79
PKSAC	11.03	574.500	Chemisorption	80
PKSAC/BVA	12.64	331.899	Chemisorption	80
MgOBi ₂	126	12.2	Chemisorption	81
AC-CSS-H ₃ P	588.24	1612	Chemisorption	This work
AC-RHS-H ₃ P	1250.00	1696	Chemisorption	This work



adsorption capacities derived from this model with the data from the literature (Table 6) highlights the remarkable performance of the materials studied. Indeed, the maximum IC retention capacities obtained, 588.24 mg g⁻¹ for AC-CSS-H₃P and 1250.00 mg g⁻¹ for AC-RHS-H₃P, are significantly higher

than those reported for other adsorbents. The high adsorption capacity of the adsorbents is attributable to their well-developed porosity and abundant surface functional groups. Moreover, this conclusion is supported by the values of the separation factor, R_L (0.7547 and 0.8696), which fall within the range of 0–1, indicating the favorable adsorption of IC onto AC-CSS-H₃P and AC-RHS-H₃P, respectively. Specifically, comparable maximum adsorption capacities have been reported in previous studies, including those by Kekes *et al.*⁷⁵ on chitosan and chitosan/ β -cyclodextrin cross-linked bead particles, Bessaha *et al.*⁷⁶ on calcined Zn/(Al + Fe) layered double hydroxides, J sica Trujillo-Reyes *et al.*²² on Fe–Ni nanostructures, and Gad *et al.*³¹ on apricot-stone-derived activated carbon, as summarized in Table 5. However, the aforementioned studies, with the exception of that of Gad *et al.*,³¹ prepared their materials for IC removal from aqueous solutions using precursors other than lignocellulosic biomass. For the Freundlich model, the obtained $1/n$ values (0.832 and 0.9048) indicate the heterogeneous surface characteristics of AC-CSS-H₃P and AC-RHS-H₃P, respectively.⁵⁵ The values of K_F (0.0799 and 0.0895 mg g⁻¹),

Table 7 Parameters of the adsorption kinetics

Kinetic model	Parameters	AC-CSS-H ₃ P	AC-RHS-H ₃ P
PFO	Q_1 (mg g ⁻¹)	9.5238	98.0392
	K_1 (min ⁻¹)	0.0171	0.2157
	R^2	0.851	0.855
PSO	Q_2 (mg g ⁻¹)	95.2381	97.0874
	K_2 (g mg ⁻¹ min ⁻¹)	0.0005	0.3536
	R^2	0.999	0.999
Elovich	B (g mg ⁻¹)	0.7658	0.5974
	α (mg g ⁻¹ min ⁻¹)	1.6362×10^{30}	8.4993×10^{23}
	R^2	0.651	0.657
Intraparticle	k_p (mg (g min ^{1/2}) ⁻¹)	0.6506	0.8353
	C (mg g ⁻¹)	91.4040	92.5320
	R^2	0.532	0.538

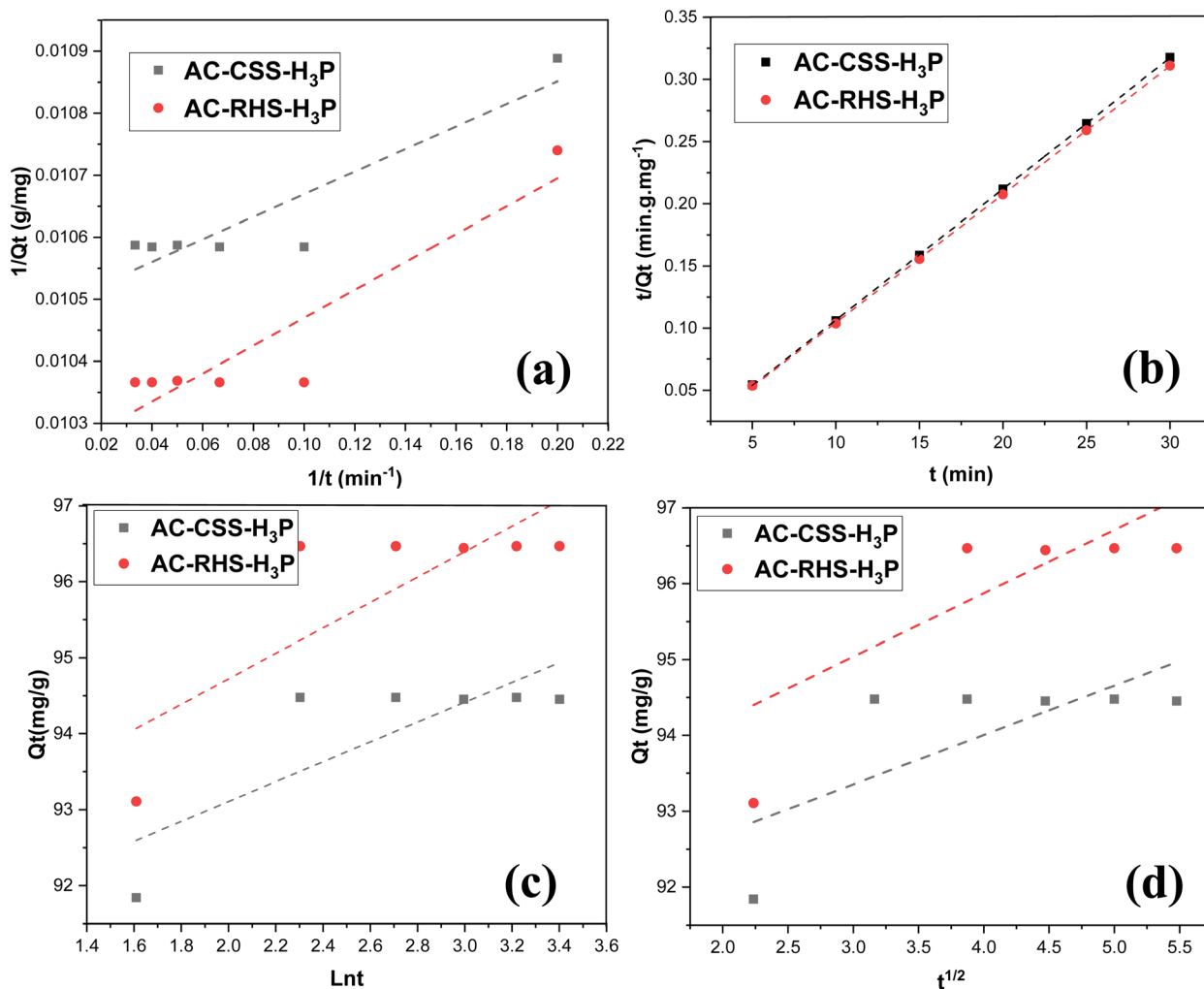


Fig. 7 Plots of the kinetics models for IC removal using AC-CSS-H₃P and AC-RHS-H₃P: (a) pseudo-first order, (b) pseudo-second order, (c) Elovich, and (d) intraparticle diffusion models.



which are related to the bonding energy, suggest that a chemisorption process occurs, further supported by the high R^2 values (>0.99) close to unity. For the Temkin and D-R models, IC adsorption onto both activated carbons shows a moderate fit, with R^2 values ranging from 0.907 to 0.9775. This finding further supports the idea of adsorption occurring at energetically heterogeneous sites.

3.4. Analysis of adsorption kinetics

The experimental data were fitted to the pseudo-first-order, pseudo-second-order, Elovich, and intraparticle diffusion kinetic models. The corresponding linear plots as a function of time are presented in Fig. 7, and the kinetic parameters are summarized in Table 7. The suitability of each kinetic model was evaluated based on the correlation coefficient (R^2), which should ideally be close to unity. The plot of t/Q_t versus t produced a straight line with an R^2 value of 0.999 for both adsorbents, indicating the excellent fit of the pseudo-second-order model to the experimental data. This finding clearly demonstrates that chemisorption is the rate-limiting step governing IC adsorption onto AC-CSS-H₃P and AC-RHS-H₃P. In this context, the adsorption process relies primarily on π - π and n - π interactions between the functional groups on the surface of the adsorbents and those of the dye. However, based on the variation in the adsorbed amount at different pH levels, it is clear

that other interactions, particularly electrostatic interactions, contribute to the adsorption process. Furthermore, hydrogen bonds are likely to form between the oxygen- and nitrogen-containing functional groups present in the molecular structure of the IC and the acidic groups present on the adsorbents, and *vice versa*. Accordingly, based on the R^2 values, the kinetic behavior of IC adsorption onto AC-CSS-H₃P and AC-RHS-H₃P follows the order: intraparticle diffusion $<$ Elovich $<$ pseudo-first-order $<$ pseudo-second-order. Fig. 8 illustrates the interactions involved in the adsorption of IC onto the activated carbons.

3.5. Regeneration test of AC-CSS-H₃P and AC-RHS-H₃P

In accordance with the observation of reduced IC adsorption under basic conditions, desorption tests were conducted using a low-concentration sodium hydroxide solution to release the adsorbed IC. Each IC-loaded adsorbent was stirred in 100 mL of a 4 mmol L⁻¹ NaOH solution for 60 min. Subsequently, the chemically regenerated adsorbent was subjected to IC adsorption again to evaluate its reusability under the same optimized conditions (initial concentration = 10 mg L⁻¹, adsorbent dose = 10 mg, pH = 4, and contact time = 15 min). As illustrated in Fig. 9, the IC removal efficiency remained nearly constant for the first three cycles and then stabilized over the final three cycles for AC-RHS-H₃P. In contrast, AC-CSS-H₃P exhibited

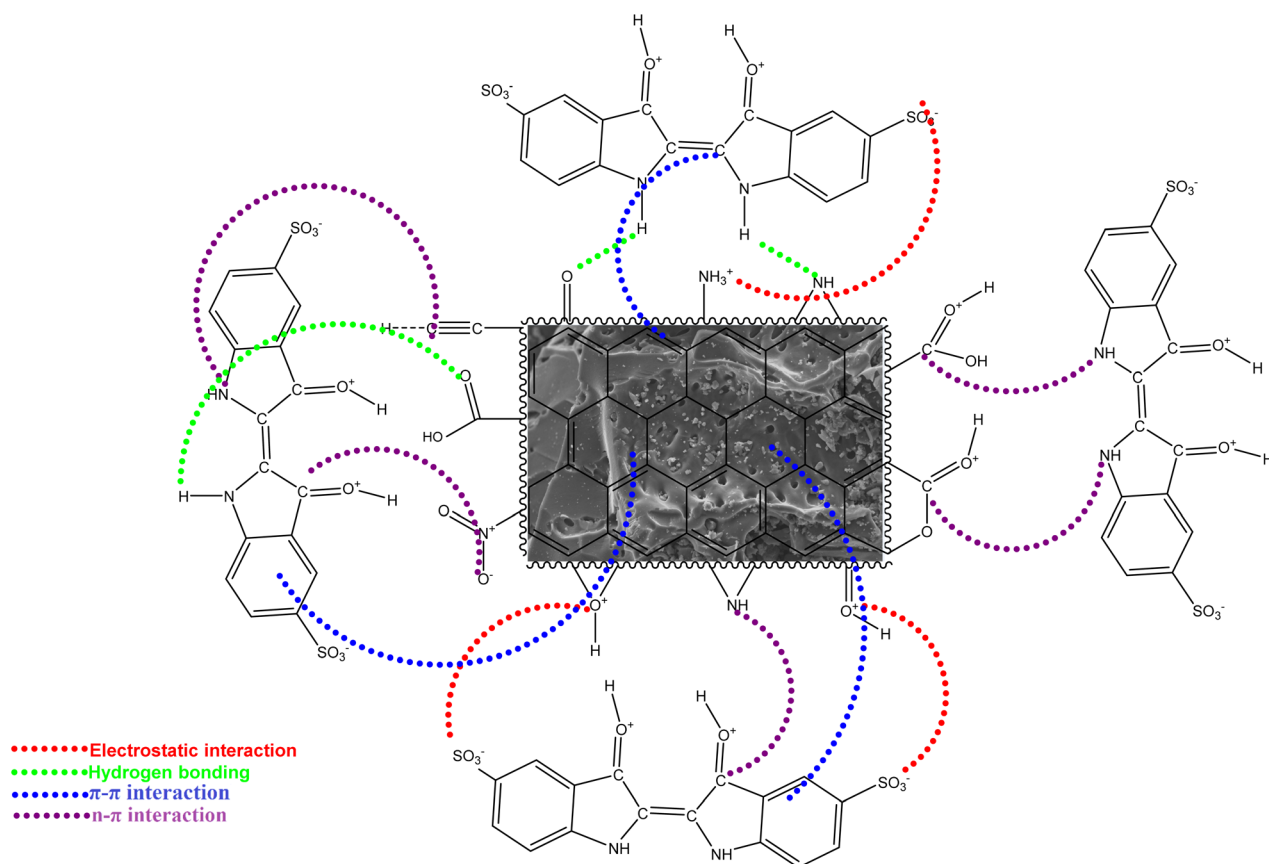


Fig. 8 Probable mechanism of the IC dye adsorption on AC-CSS-H₃P and AC-RHS-H₃P.



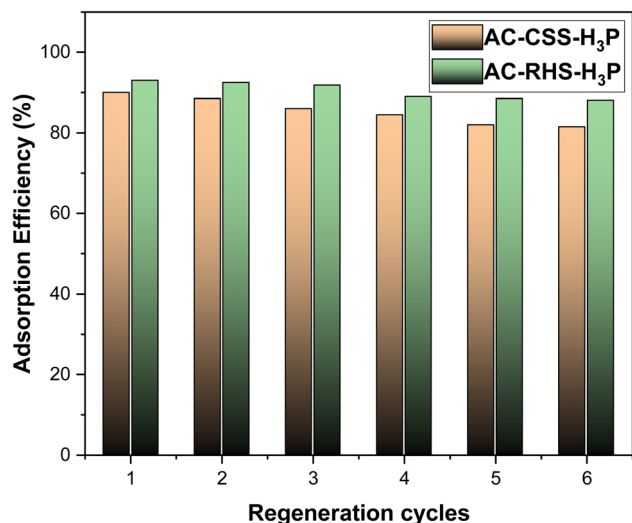


Fig. 9 Regeneration cycles of AC-CSS-H₃P and AC-RHS-H₃P.

a slight decrease in the IC removal efficiency during the first four cycles, after which performance plateaued, indicating the partial exhaustion of adsorption sites and effective regeneration. Both adsorbents maintained high adsorption efficiency, with no significant loss in performance observed after six regeneration cycles. From an economic perspective and based on the regeneration test results, these findings confirm that AC-CSS-H₃P and AC-RHS-H₃P are sustainable and low-cost adsorbents suitable for the treatment of organic dye-contaminated effluents.

4. Conclusion

This study demonstrated the suitability of CSS and RHS as effective precursors for the preparation of activated carbons and their strong adsorption capability for IC removal from aqueous solutions. The presence of abundant surface functional groups and a well-developed mesoporous structure played a key role in the high IC removal efficiencies achieved. IC adsorption was found to be unfavorable under basic conditions, whereas acidic pH significantly enhanced adsorption performance. Although all four isotherm models adequately described the equilibrium behavior, the pseudo-second-order kinetic model provided the best fit to the experimental data, indicating that chemisorption was the rate-limiting mechanism governing IC adsorption. The chemisorption process was attributed to the formation of hydrogen bonds between the oxygen and nitrogen atoms in the IC molecule and the acidic functional groups on the activated carbon surfaces. Overall, the CSS- and RHS-derived activated carbons showed excellent reusability and adsorption efficiency, confirming their potential as low-cost, sustainable adsorbents for the efficient removal of organic dyes from aqueous media.

Author contributions

Daouda Kouotou: writing – original draft, visualization, validation, resources, methodology, investigation, formal analysis,

data curation, and conceptualization. Frank Dorinel Solefack Feudjio: writing – original draft, visualization, methodology, investigation, data curation, and formal analysis. Abdelhakim Elmouwahidi, Murat Yilmaz and Julius Nsami Ndi: visualization, validation, writing – review and editing, methodology, data curation, and formal analysis. Agustin F. Perez-Cadenas and Francisco Carrasco-Marin: validation, supervision, writing – review and editing, resources, and project administration.

Conflicts of interest

The authors declare no conflicts of interest.

Data availability

Data are available on request.

Acknowledgements

The authors are grateful to the Grupo de Materiales Polifuncionales Basados en Carbono (UGR-Carbon) of the University of Granada, Spain, for the logistics provided to complete this work and the Coimbra Scholarships group for supporting the research stay.

References

- 1 Z. Wang, M. Gao, X. Li, J. Ning, Z. Zhou and G. Li, Efficient adsorption of methylene blue from aqueous solution by graphene oxide modified persimmon tannins, *Mater. Sci. Eng., C*, 2020, **108**, 110196.
- 2 X. Pang, L. Sellaoui, D. Franco, G. L. Dotto, J. Georjina, A. Bajahzar, H. Belmabrouk, A. Ben Lamine, A. Bonilla-Petriciolet and Z. Li, Adsorption of crystal violet on biomasses from pecan nutshell, para chestnut husk, araucaria bark and palm cactus: Experimental study and theoretical modeling via monolayer and double layer statistical physics models, *Chem. Eng. J.*, 2019, **378**, 122101.
- 3 P. Senthil Kumar, S. Ramalingam, C. Senthamarai, M. Niranjanaa, P. Vijayalakshmi and S. Sivanesan, Adsorption of dye from aqueous solution by cashew nut shell: Studies on equilibrium isotherm, kinetics and thermodynamics of interactions, *Desalination*, 2010, **261**, 52–60.
- 4 U. R. Lakshmi, V. C. Srivastava, I. D. Mall and D. H. Lataye, Rice husk ash as an effective adsorbent: Evaluation of adsorptive characteristics for Indigo Carmine dye, *J. Environ. Manage.*, 2009, **90**, 710–720.
- 5 A. G. S. Prado, J. D. Torres, E. A. Faria and S. C. L. Dias, Comparative adsorption studies of indigo carmine dye on chitin and chitosan, *J. Colloid Interface Sci.*, 2004, **277**, 43–47.
- 6 F. S. C. dos Anjos, E. F. S. Vieira and A. R. Cestari, Interaction of Indigo Carmine Dye with Chitosan Evaluated by Adsorption and Thermochemical Data, *J. Colloid Interface Sci.*, 2002, **253**, 243–246.
- 7 Z. Li, H. Hanafy, L. Zhang, L. Sellaoui, M. S. Netto, M. L. S. Oliveira, M. K. Seliem, G. L. Dotto, A. Bonilla-



- Petriciolet and Q. Li, Adsorption of congo red and methylene blue dyes on an ashitaba waste and a walnut shell-based activated carbon from aqueous solutions: Experiments, characterization and physical interpretations, *Chem. Eng. J.*, 2020, **388**, 124263.
- 8 N. Somsesta, V. Sricharoenchaikul and D. Aht-Ong, Adsorption removal of methylene blue onto activated carbon/cellulose biocomposite films: Equilibrium and kinetic studies, *Mater. Chem. Phys.*, 2020, **204**, 122221.
- 9 Z. Li, L. Sellaoui, G. L. Dotto, A. B. Lamine, A. Bonilla-Petriciolet, H. Hanafy, H. Belmabrouk, M. S. Netto and A. Erto, Interpretation of the adsorption mechanism of Reactive Black 5 and Ponceau 4R dyes on chitosan/polyamide nanofibers via advanced statistical physics model, *J. Mol. Liq.*, 2019, **285**, 165–170.
- 10 Z. H. Dastgerdi, S. S. Meshkat and M. D. Esrafil, Enhanced adsorptive removal of indigo carmine dye performance by functionalized carbon nanotubes-based adsorbents from aqueous solution: equilibrium, kinetic, and DFT study, *J. Nanostruct. Chem.*, 2019, **9**, 323–334.
- 11 N. Almoisheer, F. A. Alseroury, R. Kumar, M. Aslamcand and M. A. Barakat, Adsorption and anion exchange insight of indigo carmine onto CuAl-LDH/SWCNTs nanocomposite: kinetic, thermodynamic and isotherm analysis, *RSC Adv.*, 2019, **9**, 560.
- 12 J. K. Fatombi, E. A. Idohou, S. A. Ossen, I. Agani, D. Neumeyer, M. Verelst, R. Mauricot and T. Aminou, Adsorption of Indigo Carmine from Aqueous Solution by Chitosan and Chitosan/Activated Carbon Composite: Kinetics, Isotherms and Thermodynamics Studies, *Fibers Polym.*, 2019, **20**, 1820–1832.
- 13 J. Zolgharnein and M. Rastgordani, Optimization of simultaneous removal of binary mixture of indigo carmine and methyl orange dyes by cobalt hydroxide nano-particles through Taguchi method, *J. Mol. Liq.*, 2018, **262**, 405–414.
- 14 T. B. Gupta and D. H. Lataye, Adsorption of indigo carmine and methylene blue dye: Taguchi's design of experiment to optimize removal efficiency, *Sadhana*, 2018, **43**, 170.
- 15 F. Geyike, Factorial design analysis for adsorption of Indigo Carmine onto Montmorillonite-Evaluation of the kinetics and equilibrium data, *Prog. Org. Coat.*, 2016, **98**, 28–34.
- 16 T. N. Ramesh and V. P. Sreenivasa, Removal of Indigo Carmine Dye from Aqueous Solution Using Magnesium Hydroxide as an Adsorbent, *J. Mater.*, 2015, **10**, DOI: [10.1155/2015/753057](https://doi.org/10.1155/2015/753057).
- 17 T. N. Ramesh, D. V. Kirana, T. N. Mohana Kumari and A. Ashwini, Adsorption studies of indigo carmine dye by magnesium oxide, *Int. J. Sci. Res.*, 2014, **1**(4).
- 18 T. Chen, P. H. Shi, J. Zhang, Y. Li, T. Duan, L. C. Dai, L. Wang, X. F. Yu and W. K. Zhu, Natural polymer konjac glucomannan mediated assembly of graphene oxide as versatile sponges for water pollution control, *Carbohydr. Polym.*, 2018, **202**, 425–433.
- 19 C. Santhosh, V. Velmurugan, G. Jacob, S. K. Jeong, A. N. Grace and A. Bhatnagar, Role of nanomaterials in water treatment applications: a review, *Chem. Eng. J.*, 2016, **306**, 1116–1137.
- 20 Y. Dai, N. Zhang, C. Xing, Q. Cui and Q. Sun, The adsorption, regeneration and engineering applications of biochar for removal organic pollutants: a review, *Chemosphere*, 2019, **223**, 12–27.
- 21 N. O. Ankoro, D. Kouotou, P. D. B. Belibi, J. N. Ndi and J. M. Ketcha, Removal of indigo carmine (IC) by batch adsorption method onto dried cola nut shells and its active carbon from aqueous medium, *Int. J. Eng. Sci. Res. Technol.*, 2016, **5**(3), 874–887.
- 22 J. Trujillo-Reyes, M. Solache-Ríos, A. R. Vilchis-Nestor, V. Sánchez-Mendieta and A. Colín-Cruz, Fe–Ni Nanostructures and C/Fe–Ni Composites as Adsorbents for the Removal of a Textile Dye from Aqueous Solution, *Water, Air, Soil Pollut.*, 2011, **223**, 1331–1341.
- 23 N. O. Ankoro, D. Kouotou, P. K. Lunga, G. A. Tabi, R. B. N. Lekene, J. N. Ndi and J. M. Ketcha, Effect of Doping Activated Carbon Based Ricinodendron Heudelotti Shells with AgNPs on the Adsorption of Indigo Carmine and its Antibacterial Properties, *Arabian J. Chem.*, 2020, **13**(5), 5241–5253.
- 24 M. A. Ahmed, A. A. Brick and A. A. Mohamed, An efficient adsorption of indigo carmine dye from aqueous solution on mesoporous Mg/Fe layered double hydroxide nanoparticles prepared by controlled sol-gel route, *Chemosphere*, 2017, **174**, 280–288.
- 25 M. S. de Luna, R. Castaldo, R. Altobelli, G. Filippone, G. Gentile, V. Ambrogi and L. Gioiella, Chitosan hydrogels embedding hyper-crosslinked polymer particles as reusable broad-spectrum adsorbents for dye removal, *Carbohydr. Polym.*, 2017, **177**, 347–354.
- 26 S. Hashemian, B. Sadeghi and M. Mangeli, Hydrothermal synthesis of nano cavities of Al- MCF for adsorption of indigo carmine from aqueous solution, *J. Ind. Eng. Chem.*, 2015, **21**, 423–427.
- 27 M. Baysal, K. Bilge, B. Yılmaz, M. Papila and Y. Yürüm, Preparation of high surface area activated carbon from waste-biomass of sunflower piths: Kinetics and equilibrium studies on the dye removal, *J. Environ. Chem. Eng.*, 2018, **6**(2), 1702–1713.
- 28 P. C. Bhomick, A. Supong, M. Baruah, C. Pongener and D. Sinha, Pine Cone biomass as an efficient precursor for the synthesis of activated biocarbon for adsorption of anionic dye from aqueous solution: Isotherm, kinetic, thermodynamic and regeneration studies, *Sustainable Chem. Pharm.*, 2018, **10**, 41–49.
- 29 Y. Hu, X. Chen, Z. Liu, G. Wang and S. Liao, Activated carbon doped with biogenic manganese oxides for the removal of indigo carmine, *J. Environ. Manage.*, 2016, **166**, 512–518.
- 30 P. B. Wagh and V. S. Shrivastava, Removal of indigo carmine dye by using palm wood cellulose activated carbon in aqueous solution: a kinetic and equilibrium study, *International Journal of Latest Technology in Engineering, Manage. Appl. Sci.*, 2015, **4**, 106–114.
- 31 H. M. H. Gad, A. El-Hakim and A. M. Daifullah, Impact of Surface Chemistry on the Removal of Indigo Carmine Dye Using Apricot Stone Active Carbon, *Adsorpt. Sci. Technol.*, 2007, **25**(5), 327–341.



- 32 J. Zhang, P. Zhang and S. Zhang S, Comparative study on the adsorption of tetrazine and indigo carmine onto maize cob carbon, *J. Sep. Sci. Technol.*, 2014, **49**, 877–886.
- 33 Z. Harrache, M. Abbas and T. Aksil, Thermodynamic and kinetics studies on adsorption of Indigo Carmine from aqueous solution by Activated Carbon, *Microchem. J.*, 2019, **144**, 180–189.
- 34 W. L. Ang, A. W. Mohammad, A. Benamor and N. Hilal, Chitosan as natural coagulant in hybrid coagulation-nanofiltration membrane process for water treatment, *J. Environ. Chem. Eng.*, 2016, **4**, 4857–4862.
- 35 S. K. Nataraj, K. M. Hosamani and T. M. Aminabhavi, Nanofiltration and reverse osmosis thin film composite membrane module for the removal of dye and salts from the simulated mixtures, *Desalination*, 2009, **249**, 12–17.
- 36 S. F. Azha, L. Sellaoui, E. H. Engku Yunus, C. J. Yee, A. Bonilla-Petriciolet, A. Ben Lamine and S. Ismail, Iron-modified composite adsorbent coating for azo dye removal and its regeneration by photo-Fenton process: synthesis, characterization and adsorption mechanism interpretation, *Chem. Eng. J.*, 2019, **361**, 31–40.
- 37 R. Saravanan, M. M. Khan, V. K. Gupta, E. Mosquera, F. Gracia, V. Narayanan and A. Stephen, ZnO/Ag/CdO nanocomposite for visible light-induced photocatalytic degradation of industrial textile effluents, *J. Colloid Interface Sci.*, 2015, **452**, 126–133.
- 38 R. Saravanan, E. Sacari, F. Gracia, M. M. Khan, E. Mosquera and V. K. Gupta, Conducting PANI stimulated ZnO system for visible light photocatalytic degradation of coloured dyes, *J. Mol. Liq.*, 2016, **221**, 1029–1033.
- 39 F. D. S. Feudjio, C. B. D. Nguela, G. T. Kenda, D. R. T. Tchoufon, R. L. Fomekong, R. A. Ntieche, J. N. Ndi, H. M. Ngomo and C. G. Fotsop, Magnetic core-satellite Fe/Cu@ Zeolite 13X nanocomposite as an efficient catalyst: performance in indigo carmine and tetracycline degradation, *Mater. Adv.*, 2026, DOI: [10.1039/D5MA01113B](https://doi.org/10.1039/D5MA01113B).
- 40 C. Liu, H. Mao, J. Zheng and S. Zhang, Tight ultrafiltration membrane: Preparation and characterization of thermally resistant carboxylated cardo poly (arylene ether ketones) (PAEK-COOH) tight ultrafiltration membrane for dye removal, *J. Membr. Sci.*, 2017, **530**, 1–10.
- 41 Z. Huang, Y. Li, W. Chen, J. Shi, N. Zhang, X. Wang, Z. Li, L. Gao and Y. Zhang, Modified bentonite adsorption of organic pollutants of dye wastewater, *Mater. Chem. Phys.*, 2017, **202**, 266–276.
- 42 V. V. B. Rao and S. R. M. Rao, Adsorption studies on treatment of textile dyeing industrial effluent by flyash, *Chem. Eng. J.*, 2006, **116**, 77–84.
- 43 Y. Zhang, J. Liu, X. Du and W. Shao, Preparation of reusable glass hollow fiber membranes and methylene blue adsorption, *J. Eur. Ceram. Soc.*, 2019, **39**, 4891–4900.
- 44 P. Ilgin, H. Ozay and O. Ozay, Selective adsorption of cationic dyes from colored noxious effluent using a novel N-tert-butylmaleamic acid-based hydrogels, *React. Funct. Polym.*, 2019, **142**, 189–198.
- 45 A. Yazidi, L. Sellaoui, G. L. Dotto, A. Bonilla-Petriciolet, A. C. Fröhlich and A. B. Lamine, Monolayer and multilayer adsorption of pharmaceuticals on activated carbon: application of advanced statistical physics models, *J. Mol. Liq.*, 2019, **283**, 276–286.
- 46 M. Atrous, L. Sellaoui, M. Bouzid, E. C. Lima, P. S. Thue, A. Bonilla-Petriciolet and A. Ben, Lamine. Adsorption of dyes acid red 1 and acid green 25 on grafted clay: modeling and statistical physics interpretation, *J. Mol. Liq.*, 2019, **294**, 111610.
- 47 N. Laskar and U. Kumar, Removal of Brilliant Green dye from water by modified Bambusa Tulda: adsorption isotherm, kinetics and thermodynamics study, *Int. J. Environ. Sci. Technol.*, 2019, **16**, 1649–1662.
- 48 M. Danish and T. Ahmad, A review on utilization of wood biomass as a sustainable precursor for activated carbon production and application, *Renewable Sustainable Energy Rev.*, 2018, **87**, 1–21.
- 49 A. Wahabou, A. N. Rahman, D. Kouotou and A. Paltahé, Adsorption of congo red on activated carbon modified by plasma, *Int. J. Eng. Sci. Res. Technol.*, 2017, **5**(1), 30–43.
- 50 A. M. Kammegne, J. N. Ndi, D. Kouotou, R. N. Che, P. D. B. Belibi, N. O. Ankoru, B. Z. Zing and J. M. Ketcha, Activated carbon based Canarium Schweinfurthii shells for the removal of nitrate ions from aqueous solution, *Int. J. Eng. Sci. Res. Technol.*, 2017, **6**(7), 805–815.
- 51 A. M. Kammegne, J. N. Ndi, D. Kouotou, R. N. Che and J. M. Ketcha, Adsorption Study of the Removal of Copper (II) Ions using Activated Carbon Based Canarium Schweinfurthii Shells Impregnated with ZnCl₂, *IRA-Int. J. Appl. Sci.*, 2017, **8**(1), 18–30.
- 52 D. Kouotou, H. Ngomo Manga, A. Baçaoui, A. Yaacoubi and J. Ketcha Mbadcam, Optimization of Activated Carbons prepared by H₃PO₄ and Steam Activation of Oil Palm Shells, *J. Chem.*, 2013, **2013**, 10.
- 53 D. Kouotou, H. Ngomo Manga, A. Baçaoui, A. Yaacoubi and J. Ketcha Mbadcam, Physicochemical Activation of Oil Palm Shells using Response surface Methodology: Optimization of Activated Carbons Preparation, *Int. J. Curr. Res.*, 2013, **5**(3), 431–438.
- 54 I. Langmuir, The adsorption of gases on plane surfaces of glass, mica and platinum, *J. Am. Chem. Soc.*, 1918, **40**, 1361–1403.
- 55 H. M. F. Freundlich, Over the adsorption in solution, *J. Phys. Chem.*, 1906, **57**, 385–470.
- 56 C. H. Yang, Statistical mechanical study on the Freundlich isotherm equation, *J. Colloid Interface Sci.*, 1998, **208**, 379–387.
- 57 M. J. Temkin and V. Pyzhev, Recent modifications to Langmuir isotherms, *Acta Physicochim. URSS*, 1940, **12**, 217–225.
- 58 M. M. Dubinin and L. V. Radushkevich, Equation of the characteristic curve of activated charcoal, *Chem. Zentralbl.*, 1947, **1**, 875.
- 59 N. D. Hutson and R. T. Yang, Theoretical basis for the Dubinin–Radushkevitch (D–R) adsorption isotherm equation, *Adsorption*, 1997, **3**, 189–195.
- 60 T. W. Weber and R. K. Chakravorti, Pore and solid diffusion models for fixed-bed adsorbents, *AIChE J.*, 1974, **20**, 228–238.



- 61 S. Lagergren, About the theory of so-called adsorption of soluble substances, *Kungliga Svenska Vetensk Handl.*, 1898, vol. 24, pp. 1–39.
- 62 Y. S. Ho, Citation review of Lagergren kinetic rate equation on adsorption reactions, *Scientometrics*, 2004, **59**, 171–177.
- 63 Y. S. Ho and G. McKay, Pseudo-second order model for sorption processes, *Process Biochem.*, 1999, **34**, 451–465.
- 64 Y. S. Ho, Review of second-order models for adsorption systems, *J. Hazard. Mater.*, 2006, **136**, 681–689.
- 65 S. Azizian, Kinetic models of sorption: a theoretical analysis, *J. Colloid Interface Sci.*, 2004, **276**, 47–52.
- 66 W. J. Weber and J. C. Morris, Kinetics of adsorption on carbon from solution, *J. Sanit. Eng. Div., Am. Soc. Civ. Eng.*, 1963, **89**, 31–60.
- 67 N. Álvarez-Gutiérrez, M. V. Gil, F. Rubiera and C. Pevida, Cherry-stones-based activated carbons as potential adsorbents for CO₂/CH₄ separation: effect of the activation parameters, *Greenhouse Gases:Sci. Technol.*, 2015, **5**(6), 812–825.
- 68 A. J. Tsamba, W. Yang and W. Blasiak, Pyrolysis characteristics and global kinetics of coconut and cashew nut shells, *Fuel Process. Technol.*, 2006, **87**, 523–530.
- 69 M. Thommes, K. Kaneko, A. V. Neimark, J. P. Olivier, F. Rodriguez-Reinoso, J. Rouquerol and K. S. W. Sing, Physisorption of gases, with special reference to the evaluation of surface area and pore size distribution (IUPAC Technical Report), *Pure Appl. Chem.*, 2015, **87**(9–10), 1051–1069.
- 70 M. El Hajam, N. Idrissi Kandri, A. Harrach, A. El khomsi and A. Zerouale, Adsorption of Methylene Blue on industrial softwood waste "Cedar" and hardwood waste "Mahogany": comparative study, *Mater. Today: Proc.*, 2019, **13**, 812–821.
- 71 M. Abbas, Z. Harrache, T. Aksil and M. Trari, Removal of indigo carmine (IC) in aqueous solution onto activated pomegranate peel (APP) by adsorption process: Kinetic and thermodynamic studies, *J. Eng. Fibers Fabr.*, 2021, **17**, 1–10.
- 72 A. Mittal, J. Mittal and L. Kurup, Utilization of hen feathers for the adsorption of Indigo Carmine from simulated effluents, *J. Environ. Prot. Sci.*, 2007, **1**, 92–100.
- 73 V. K. Gupta, R. Kumar, A. Nayak, T. A. Saleh and M. A. Barakat, Review article; adsorptive removal of dyes from aqueous solution onto carbon nanotubes: a review, *Adv. Colloid Interface Sci.*, 2013, **193**, 24–34.
- 74 C. Namasivayam and D. Kavitha, Removal of congo red from water by adsorption onto activated carbon prepared from coir pith, an agricultural solid waste, *Dyes Pigm.*, 2002, **54**, 47–58.
- 75 T. Kekes and C. Tzia, Adsorption of indigo carmine on functional chitosan and β -cyclodextrin/chitosan beads: Equilibrium, kinetics and mechanism studies, *J. Environ. Manage.*, 2020, **262**, 110372.
- 76 H. Bessaha, M. Bouraada and L. C. Deménorval, Removal of indigo carmine and green bezanyl- F2B from water using Calcined and Uncalcined Zn/Al + Fe layered double hydroxide, *J. Water Reuse Desalin.*, 2017, **7**(2), 152–161.
- 77 M. Li, H. Wang and S. Wu, Adsorption of hazardous dyes indigo carmine and acid red on nanofiber membranes, *RSC Adv.*, 2012, **1**(3), 900–907.
- 78 T. B. Gupta and D. H. Lataye, Adsorption of Indigo Carmine Dye onto Acacia Nilotica (Babool) Sawdust Activated Carbon, *J. Hazard. Toxic Radioact. Waste*, 2017, **21**(4), DOI: [10.1061/\(ASCE\)HZ.2153-5515.0000365](https://doi.org/10.1061/(ASCE)HZ.2153-5515.0000365).
- 79 N. Y. Elamin, Indigo carmine pigment adsorption utilizing MgO nanostructures fabricated from pimpinella anisum extract, *J. Optoelectron. Biomed. Mater.*, 2022, **14**(3), 115–127.
- 80 G. A. Tabi, R. B. N. Lekene, D. Kouotou, N. O. Ankoro, A. V. Abéga, J. N. Ndi and J. M. Ketcha, Nonlinear modelling of the adsorption of indigo carmine dye from wastewater onto characterized activated carbons/volcanic ash composite, *Arabian J. Chem.*, 2022, **15**, 103515.
- 81 F. A. Adam, M. G. Ghoniem, M. Diawara, S. Rahali, B. Y. Abdulkhair, M. R. Elamin, M. A. B. Aissa and M. Seydou, Enhanced adsorptive removal of indigo carmine dye by bismuth oxide doped MgO based adsorbents from aqueous solution: equilibrium, kinetic and computational studies, *RSC Adv.*, 2022, **12**(38), 24786–24803.

